

# Bradycardic onset of spiral wave re-entry: structural substrates

Christian W. Zemlin\* and Arkady M. Pertsov

Department of Pharmacology, SUNY Upstate Medical University, Syracuse, NY 13210, USA

## KEYWORDS

Arrhythmia onset;  
Bradycardia;  
Spiral wave;  
Structural substrate;  
Atrial fibrillation

**Aims** The least understood aspect of re-entrant cardiac arrhythmias is how they start spontaneously. The known mechanisms for re-entry induction involve the application of premature electrical stimuli or rapid pacing, whereas in a clinical setting, re-entry often occurs at normal heart rates. Here, we propose a physiological mechanism of re-entry onset at normal and slow heart rates, which is based on structurally determined heterogeneities.

**Methods and results** Using a two-dimensional tissue model with Luo–Rudy II kinetics, we study electrical propagation in the presence of macroscopic coupling heterogeneities. We find that spiral wave re-entry occurs if steep and smooth coupling gradients are situated side by side, with the critical steepness depending on the frequency of stimulation. We demonstrate how bradycardia can unmask a slow endogenous pacemaker in a poorly coupled region, subsequently leading to spiral wave re-entry.

**Conclusion** In the presence of coupling heterogeneities, a single excitation coming from the less coupled region may induce spiral wave re-entry.

## Introduction

Re-entrant waves of cardiac activity are an important cause of tachyarrhythmias. They have been observed experimentally in a variety of species, including dog,<sup>1</sup> pig,<sup>2</sup> rabbit,<sup>3</sup> guinea pig,<sup>4</sup> and human,<sup>5,6</sup> and in different parts of the heart, including the ventricles,<sup>6</sup> the atrial free wall,<sup>4</sup> the pulmonary veins,<sup>7,8</sup> and the AV node.<sup>9</sup> Dynamics of re-entrant waves has been studied extensively. Little is known, however, about the initiation of re-entrant waves *in vivo*. Currently considered initiation mechanisms rely on the creation of a phase singularity<sup>10</sup> or 'critical point',<sup>11</sup> i.e. a point around which a spiral wave can revolve. Phase singularities can be created by applying a strong electric field,<sup>11</sup> a strong electrical stimulus during the vulnerable window,<sup>12</sup> or by a train of ectopic beats leading to discordant alternans.<sup>13</sup> In a clinical setting, however, re-entrant arrhythmias often occur following normal heart rates or during bradycardia or pause,<sup>14,15</sup> and there is no mechanism known to explain this phenomenon.

Here, we describe a mechanism that can explain the bradycardic onset of spiral wave re-entry. Our mechanism assumes the presence of structural heterogeneities, involving abrupt changes in tissue coupling ('source–sink mismatch'<sup>16</sup>) as well as a latent pacemaker located in a low coupling region. Source–sink mismatch and unidirectional propagation have been studied computationally<sup>17</sup> and

experimentally in strands of cardiac myocytes with abruptly changing width.<sup>16</sup>

We demonstrate that in two dimensions, source–sink mismatch gives rise to spontaneous initiation of spiral wave re-entry from a single propagating excitation wave originating from a latent pacemaker. We start by identifying conditions under which source–sink mismatch occurs in the Luo–Rudy dynamic model of cardiac myocytes. Then, we study the geometrical conditions under which our mechanism can be realized. We discuss its clinical relevance in various scenarios, including the induction of atrial fibrillation in the pulmonary veins.

## Methods

We use standard reaction–diffusion equations to describe the propagation of electrical excitation:

$$C_m \frac{\partial V}{\partial t} = -(I_{ion}(V, \vec{x}) + I_{stim}) + \nabla \cdot (\sigma \nabla V)$$
$$\frac{\partial \vec{x}}{\partial t} = f(V, \vec{x}) \quad (1)$$

where  $C_m$  is the specific capacitance of the cell membrane,  $V$  the transmembrane voltage,  $I_{ion}$  the total ionic current across the membrane,  $\vec{x}$  a vector containing all variables besides  $V$  that are used to describe the local state of the medium (including ion concentrations and gating variables),  $I_{stim}$  the stimulus current,  $\sigma$  the local conductivity tensor describing the coupling between cells, and  $f$  a function describing the dynamics of all variables except  $V$ .

The electrophysiological properties of the tissue are modelled according to the ventricular guinea pig model of Luo and Rudy in

\* Corresponding author. Tel: +1 315 464 7988; fax: +1 315 464 8014.  
E-mail address: zemlinc@upstate.edu

its latest version.<sup>18</sup> Equation (1) was solved using an Euler scheme with a space step of 200  $\mu\text{m}$  and a time step of 20  $\mu\text{s}$ . To pace tissue at a certain location, we increased  $I_{\text{stim}}$  for 2 ms from 0 to twice the threshold value required to induce excitation.

To determine the conditions under which source–sink mismatch occurs, we simulated a one-dimensional cable of length 8 cm with spatially variable coupling (as shown in *Figure 1A* and *D*). To determine the rate dependence of conduction block, we used a ramping stimulation protocol, starting at a basic cycle length (BCL) of 600 ms and then reducing the BCL in steps of 5 ms after every five pulses.

The two-dimensional simulations were conducted in a 20 mm  $\times$  6 mm sheet. We describe cell coupling by a diagonal conductivity tensor,

$$\sigma(x, y) = \begin{pmatrix} \sigma_x(x, y) & 0 \\ 0 & \sigma_y(x, y) \end{pmatrix}$$

and assume that the coupling is normal in one part of the tissue but reduced in the other part. The precise distribution of conductivities used in our simulations is given by a two-dimensional Boltzmann distribution:

$$\sigma_x(x, y) = \sigma_{\min} + \frac{(\sigma_{\max} - \sigma_{\min})}{(1 + \exp[-(k_y \max + (k_y \min - k_y \max)/(1 + \exp[-k_x(x - x_{\text{crit}})]))](y - y_{\text{crit}}))} \quad (2)$$

where  $\sigma_{\min}$  and  $\sigma_{\max}$  are the minimum and the maximum conductivities,  $\sigma_{y,\min}$  and  $\sigma_{y,\max}$  the minimal and the maximal characteristic lengths over which the transition from reduced to normal coupling occurs in  $y$ -direction, and  $k_x$  the characteristic length over which the transition from abrupt to smooth in  $y$ -direction occurs in  $x$ -direction. The values used in our simulations were  $\sigma_{\min} = 0.081 \text{ S/m}$ ,  $\sigma_{\max} = 1.08 \text{ S/m}$ ,  $k_x = 3.3/\text{mm}$ ,  $k_{y,\min} = 0.825/\text{mm}$ ,  $k_{y,\max} = 330/\text{mm}$ ,  $x_{\text{crit}} = 12 \text{ mm}$ , and  $y_{\text{crit}} = 6.7 \text{ mm}$ .

We simulated an endogenous pacemaker in our medium by reducing  $I_{K1}$  to 0 in a square of side 1.6 mm around the lower left-hand corner; at the same time, we reduced the coupling in this area to  $\sigma = 0.027 \text{ S/m}$ .

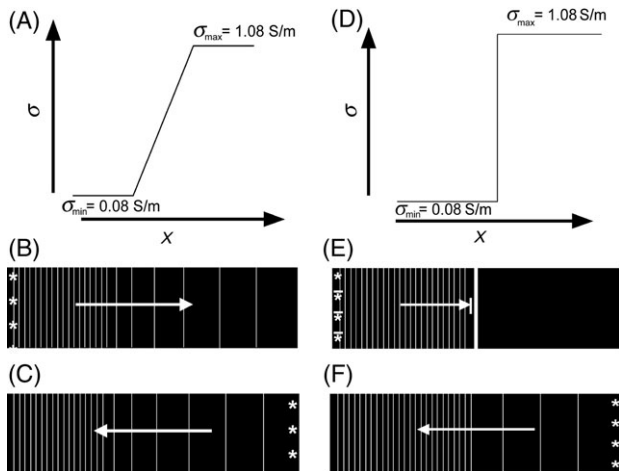


**Figure 1** Wave propagation across a smooth rise (*A–C*) and a steep rise (*D–F*) in coupling. (*A*) Coupling as a function of  $x$ . (*B*) Activation sequence for stimulation at the reduced coupling end. Stars mark the line of stimulation; thin lines are isochrones, spaced 10 ms apart. The arrow indicates the direction of propagation. (*C*) Propagation for stimulation at the normal coupling end. (*D*) Coupling profile with steep gradient. (*E*) Conduction block for propagation from reduced to normal coupling region (due to source–sink mismatch). (*F*) Successful propagation from normal to reduced coupling region.

## Results

The phenomenon of source–sink mismatch in a stripe of excitable tissue with variable coupling is illustrated in *Figure 1*. *Figure 1A–C* shows the case of a smooth transition of coupling (from  $\sigma_{\min} = 0.08 \text{ S/m}$  to  $\sigma_{\max} = 1.08 \text{ S/m}$ ). The activation pattern is independent of the direction of propagation, despite significant asymmetry in coupling.

The situation changes dramatically when the transition of coupling becomes sufficiently steep (*Figure 1D–F*). Now the transition from  $\sigma_{\min}$  to  $\sigma_{\max}$  occurs over 200  $\mu\text{m}$  rather than 5 mm. The steep transition causes source–sink mismatch at the junction and failure of excitation waves to penetrate into the region of normal coupling (*Figure 1E*). Waves originating in the normal coupling region, however, propagate across the junction as before (compare *C* and *F*).

The block caused by source–sink mismatch is frequency-dependent. *Figure 2* shows how the critical pacing period at which block occurs ( $\text{BCL}_c$  or  $\text{BCL}_{\text{crit}}$ ) depends on the ratio of coupling  $r = \sigma_{\max}/\sigma_{\min}$ . One can identify three domains of conduction: complete block for very fast stimulation (marked in dark grey), bidirectional propagation for sufficiently low coupling ratios and sufficiently high BCLs (white), and unidirectional block in between (marked in light grey).

For  $r \approx 1$ , unidirectional block can be achieved only at short BCLs. As the conduction ratio increases, the range of BCLs leading to unidirectional block slowly increases, until at a finite value ( $r \approx 13$ ), there is unidirectional block for any stimulating BCL. Unidirectional block for  $\text{BCL} < \text{BCL}_c$  is not permanent but of the Wenckebach type. *Figure 3A* shows an example of time-dependent unidirectional block at the transition from low to high coupling. The distribution of conductivities (*Figure 3A*) has two intermediate steps between  $\sigma_{\min}$  and  $\sigma_{\max}$ . It allows bidirectional propagation at  $\text{BCL} = 300 \text{ ms}$ , but exhibits unidirectional block at  $\text{BCL} = 180 \text{ ms}$ . *Figure 3B* shows recordings from both the

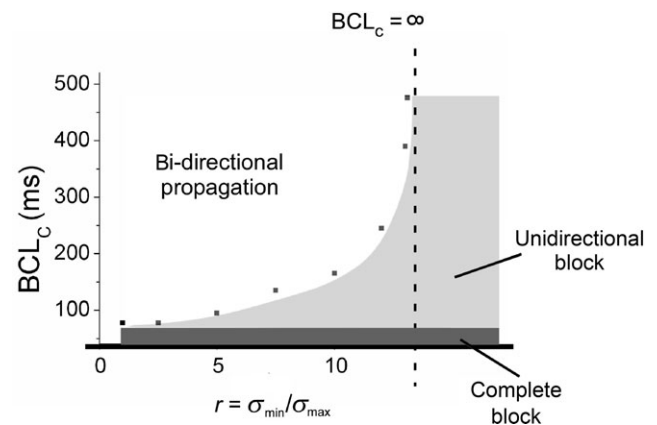


**Figure 2** Frequency dependence of conduction block. A one-dimensional medium with coupling distribution, as shown in *Figure 1D*, but with variable  $\sigma_{\min}$ , is periodically stimulated at the poorly conducting end ( $\sigma_{\max}$  remains constant). The dots in the figure mark for each value of  $\sigma_{\min}/\sigma_{\max}$ , the minimum stimulation BCL that is conducted across the transition in coupling in a 1:1 manner. The dashed line marks the value of  $\sigma_{\min}/\sigma_{\max}$ , above which there is a unidirectional block independent of stimulation BCL. The light grey area indicates where in our parameter space unidirectional block occurs and the dark grey area the region of complete block.

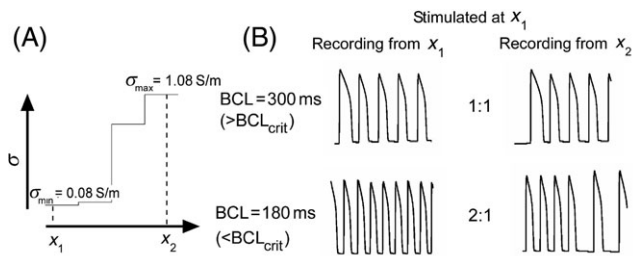


**Figure 3** Wenckebach rhythms at the transition site of conductivities. (A) Coupling profile; (B) conduction patterns for two different stimulation BCLs (300 and 180 ms). Left column shows activation at  $x_1$  and right column activity at  $x_2$ . All traces were obtained by gradually decreasing BCL (see Methods). For BCL = 180 ms, 2:1 conduction does not occur immediately but develops after four beats have been conducted in a 1:1 manner.

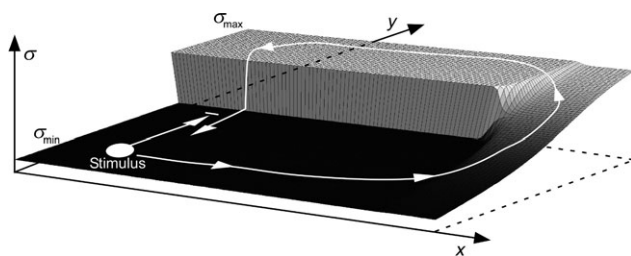


**Figure 4** Schematic of re-entry induction at a heterogeneous transition from reduced coupling ( $\sigma_{\min}$ ) to normal coupling ( $\sigma_{\max}$ ).

reduced and the normal coupling part of the medium for stimulation at each of the frequencies. The reduced coupling part ( $x_1$ ) responds to each stimulus for both frequencies. The normally conducting part ( $x_2$ ) responds in a 1:1 fashion for stimulation at BCL = 300 ms; for stimulation at BCL = 180 ms, it only conducts four beats until 2:1 conduction sets in (2:1 conduction is stable).

In a two-dimensional medium, a supercritical transition from low to high coupling can form a substrate for the bradycardic onset of spiral wave re-entry. A schematic of such a substrate is shown in *Figure 4*. The characteristic feature is an area of good conduction next to an area of poor conduction, with a transition of variable steepness. In the left part of the medium, the transition is supercritical, so that waves coming from the reduced conduction area are blocked. At the right border of the medium, the transition is subcritical, so that excitation can propagate in both directions [the distribution of conductivities is given in Eq. (2)].

A stimulus originating in the reduced coupling region can initiate re-entry. Inside the reduced coupling region, the stimulus can propagate in all directions. When it reaches the interface with the well-conducting region, it is blocked in the left part but propagates towards the right edge, where it can continue into the upper part of the medium. In the upper part, the wave propagates from the right to the left and then downwards to close the re-entry loop.

*Figure 5* shows bradycardic onset of spiral wave re-entry in the Luo–Rudy model of ventricular cardiac tissue. We used the distribution of conductivities shown in *Figure 4* and constructed an endogenous pacemaker in the lower left corner of the medium (see Methods). *Figure 5A–C* shows a sinus beat, which we simulate by injecting current along

the normally conducting border of our medium (at the top). The sinus beat of excitation traverses the medium and resets the endogenous pacemaker; the pacemaker will remain ineffective as long as the sinus rhythm is faster than its natural frequency.

After the sinus beat shown in *Figure 5A–C* had passed, we deliberately increased the sinus BCL (from 600 to 900 ms) to above the frequency of the endogenous pacemaker (the pacemaker initially activates after  $\sim 800$  ms). As a consequence, the endogenous pacemaker generates an ectopic beat (*Figure 5D*). This beat propagates rightward in the reduced coupling region (*Figure 5E*), but cannot propagate into the normally conducting region due to source–sink mismatch. As the wave reaches the smooth coupling transition on the right side of the medium (*Figure 5F*), the next sinus wave arrives and the two waves annihilate (*G*).

The subsequent ectopic beat starts out as the first one (*Figure 5H and I*), but this time, the wave enters into the normally conducting region before the sinus beat arrives (note that as the pacemaker was not reset by sinus rhythm in the first ectopic beat, the time difference between second ectopic beat and corresponding sinus beat should be twice that between first ectopic beat and corresponding sinus beat). Consequently, spiral wave re-entry forms (*Figure 5J and K*) and persists until the sinus rhythm annihilates it (as in *F*) or until the spiral wave drifts to the boundary.

Traces (a–c) are recorded during re-entry induction from the locations marked in *Figure 5A*. Trace (a) is recorded from the endogenous pacemaker. The first action potential represents the last sinus beat. The next to action potential are ectopic beats (note the characteristic slow depolarization). The second ectopic beat is followed by a rapid burst of eight activations, produced by the spiral wave re-entry.

Traces (b) and (c) are reminiscent of early afterdepolarizations (EADs). Although EADs are usually attributed to abnormal intracellular calcium handling,<sup>19–22</sup> our model suggests that the observation of ‘EADs’ could also be the result of re-entry. In our case, they are purely a result of the incomplete repolarization that occurs at the centre of a re-entrant wave. As the re-entrant wave drifts, the affected area also drifts. In our example, location (b) is affected right at the beginning, whereas location (c) is affected in the second action potential.

## Discussion

We have described a mechanism for spiral wave re-entry initiation during bradycardia. The mechanism relies only on a structural substrate composed of neighbouring regions of different coupling and a varying steepness of the transition between them. In such a situation, a single excitation coming from the less conducting region can induce spiral wave re-entry.

Previous studies have initiated re-entry either by applying a strong stimulus in the vulnerable period of a wave, by applying a strong electric field,<sup>11</sup> or by delivering a train of ectopic beats.<sup>13</sup> In all these mechanisms, wave breaks are created by the interaction of sinus beats with additionally applied beats or fields. However, tachyarrhythmias occur also following bradycardia or pause,<sup>14,15</sup> in which such an interaction is unlikely or even impossible. The mechanism

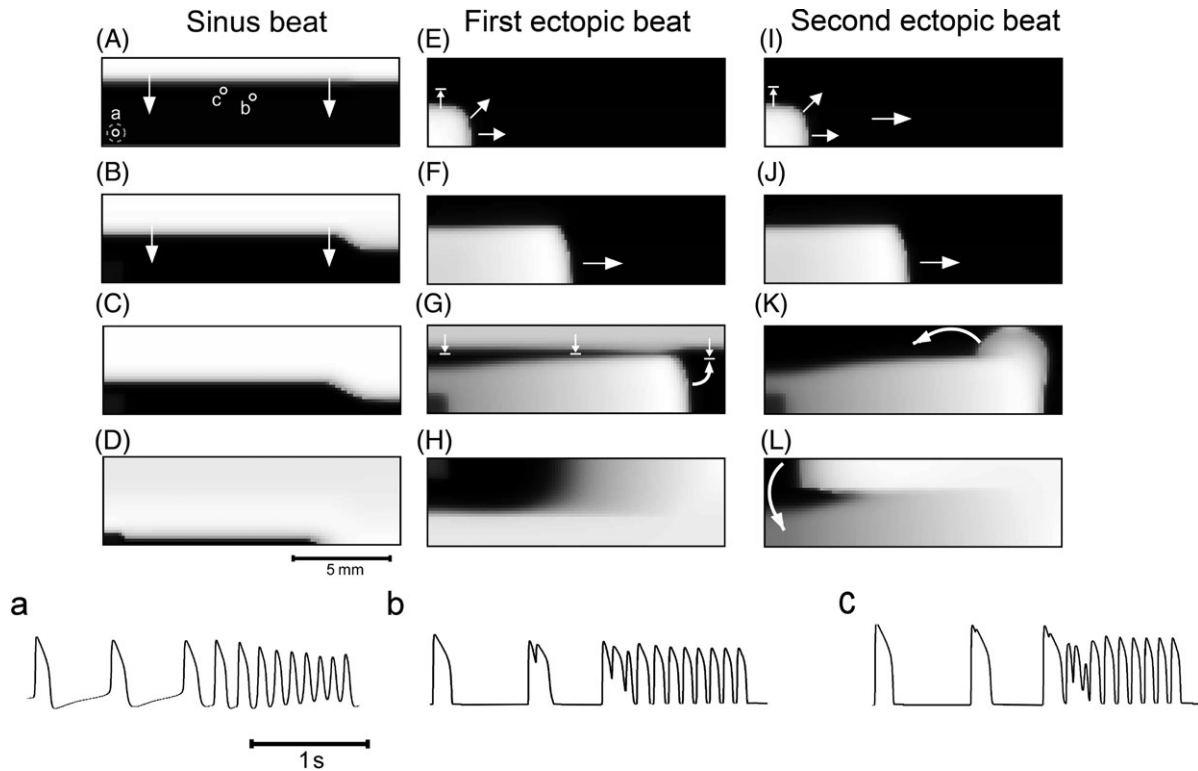


**Figure 5** Bradycardic onset of spiral wave re-entry. (A–D) Propagation of the last sinus wave at normal frequency. White areas represent excited medium, whereas black areas represent resting medium. Letters in (A) indicate points for which electrical signal is shown below. Dashed grey circle marks position of endogenous pacemaker. (E) First ectopic beat from the reduced coupling domain. (F) The wave propagates leftwards, but cannot propagate upwards. (G) The first bradycardic sinus beat arrives as the wave is about to turn. Both the ectopic and the sinus wave are annihilated. (I and J) The second ectopic beat is initiated and propagates leftwards. (K and L) Formation of a re-entrant wave. (a–c) Recordings of the electrical activity from the locations marked in (A).

described here does not rely on the interaction of waves, but explains the induction of spiral wave re-entry purely from the interaction of a normally propagating wave with a structural substrate.

The structural substrates needed for our spiral wave induction mechanism are likely present in several parts of the heart. Indeed, it has been reported that electrical conduction in the myocardial sleeves of pulmonary veins is highly heterogeneous.<sup>7,23</sup> Similar substrates can be expected to occur in other regions in the heart where excitable tissue fades out, such as tissue at the atrio-ventricular boundary or at the border zone of a myocardial infarction. The other main ingredient required for our mechanism is a single ectopic beat. In our mechanism, the ectopic beat does not have to occur spontaneously; if the natural frequency of an ectopic pacemaker is lower than that of the sinus node, such a pacemaker can be present over a long time without becoming visible. A bradycardic event during which the sinus frequency drops below that of the pacemaker can suffice to let the ectopic pacemaker emit one stimulus and induce re-entry. Automaticity in the pulmonary veins has been described<sup>24</sup> and typically occurs with a frequency below that of the sinus node.<sup>25</sup>

The initiation of atrial fibrillation in the pulmonary veins is the most likely clinical application of the mechanism. As there is evidence for the presence of all ingredients of our mechanism in the pulmonary veins and they are at the same time known to play a crucial role in the initiation of

atrial fibrillation, it would be most promising to try to establish that our mechanism is at work there. If the sinus node could be selectively slowed down or uncoupled during electrophysiological testing, this may demonstrate the presence of a latent pacemaker in the pulmonary veins. Such a procedure to localize the cause of re-entry at least in part of the patients may improve the effectiveness of therapies such as the ablation of arrhythmogenic tissue.

Although we demonstrated re-entry induction for a particular generic geometry, the mechanism is equally effective for a large class of substrates. For example, the spatial dimensions of the line of block do not have to be as large as the 16 mm used in our model. If coupling in the poorly conducting region is further reduced, say to 1% of the normal value (in this article, we used a reduction to 7%), the line of block only needs to be 3 mm long, and the needed line of block shrinks further as the coupling in the poorly conducting region decreases. Such a reduction may seem enormous, but reductions of conduction speed to ~10%, corresponding to 1% coupling, have been reported by several studies for the pulmonary veins.<sup>7,23</sup> It should also be kept in mind that we are considering structural pathologies that only occur in a fraction of all patients.

The main limitation of this study is that we used a simplified geometry and idealized distribution of conductivities. More detailed simulation studies and experiments are required whether or not real substrates support the mechanism described.

**Conflict of interest:** none declared.

## Funding

Research for this article was supported by NIH grants RO1-HL071762-01A1 and RO1-HL071635-01.

## References

1. Wu J, Wu J, Olgin J, Miller JM, Zipes DP. Mechanisms underlying the reentrant circuit of atrioventricular nodal reentrant tachycardia in isolated canine atrioventricular nodal preparation using optical mapping. *Circ Res* 2001;**88**:1189–95.
2. Baxter WT, Mironov SF, Zaitsev AV, Jalife J, Pertsov AM. Visualizing excitation waves inside cardiac muscle using transillumination. *Biophys J* 2001;**80**:516–30.
3. Efimov IR, Cheng Y, Van Wagoner DR, Mazgalev T, Tchou PJ. Virtual electrode-induced phase singularity: a basic mechanism of defibrillation failure. *Circ Res* 1998;**82**:918–25.
4. Samie FH, Berenfeld O, Anumonwo J, Mironov SF, Udassi S, Beaumont J *et al*. Rectification of the background potassium current: a determinant of rotor dynamics in ventricular fibrillation. *Circ Res* 2001;**89**:1216–23.
5. Nanthakumar K, Jalife J, Masse S, Downar E, Pop M, Asta J *et al*. Optical mapping of Langendorff perfused human hearts: establishing a model for the study of ventricular fibrillation in humans. *Am J Physiol Heart Circ Physiol*, Published online ahead of print 2007.
6. Nash MP, Mourad A, Clayton RH, Sutton PM, Bradley CP, Hayward M *et al*. Evidence for multiple mechanisms in human ventricular fibrillation. *Circulation* 2006;**114**:536–42.
7. Arora R, Verheule S, Scott L, Navarrete A, Katari V, Wilson E *et al*. Arrhythmogenic substrate of the pulmonary veins assessed by high-resolution optical mapping. *Circulation* 2003;**107**:1816–21.
8. Po SS, Li Y, Tang D, Liu H, Geng N, Jackman WM *et al*. Rapid and stable re-entry within the pulmonary vein as a mechanism initiating paroxysmal atrial fibrillation. *J Am Coll Cardiol* 2005;**45**:1871–7.
9. Moe GK, Preston JB, Burlington H. Physiologic evidence for a dual A-V transmission system. *Circ Res* 1956;**4**:357–75.
10. Winfree AT. *When Time Breaks Down: The Three-Dimensional Dynamics of Electrochemical Waves and Cardiac Arrhythmias*. Princeton, NJ: Princeton University Press; 1987.
11. Frazier DW, Wolf PD, Wharton JM, Tang AS, Smith WM, Ideker RE. Stimulus-induced critical point mechanism for electrical initiation of reentry in normal canine myocardium. *J Clin Invest* 1989;**83**:1039–52.
12. Hoffman B, Suckling EE, Brooks CM. Vulnerability of the dog ventricle and effects of defibrillation. *Circ Res* 1955;**3**:147–51.
13. Gong Y, Xie F, Stein KM, Garfinkel A, Cuiianu CA, Lerman BB *et al*. Mechanism underlying initiation of paroxysmal atrial flutter/atrial fibrillation by ectopic foci: a simulation study. *Circulation* 2007;**115**:2094–102.
14. Dimmer C, Szili-Torok T, Tavernier R, Verstraten T, Jordaens LJ. Initiating mechanisms of paroxysmal atrial fibrillation. *Europace* 2003;**5**:1–9.
15. Schwartzman D, Blagev DP, Brown ML, Mehra R. Electrocardiographic events preceding onset of atrial fibrillation: insights gained using an implantable loop recorder. *J Cardiovasc Electrophysiol* 2006;**17**:243–6.
16. Rohr S, Kucera JP, Fast VG, Kleber AG. Paradoxical improvement of impulse conduction in cardiac tissue by partial cellular uncoupling. *Science* 1997;**275**:841–4.
17. Rudy Y. Reentry: insights from theoretical simulations in a fixed pathway. *J Cardiovasc Electrophysiol* 1995;**6**:294–312.
18. Faber GM, Rudy Y. Action potential and contractility changes in overloaded cardiac myocytes: a simulation study. *Biophys J* 2000;**78**:2392–404.
19. Burashnikov A, Antzelevitch C. Reinduction of atrial fibrillation immediately after termination of the arrhythmia is mediated by late phase 3 early afterdepolarization-induced triggered activity. *Circulation* 2003;**107**:2355–60.
20. Burashnikov A, Antzelevitch C. Late-phase 3 EAD. A unique mechanism contributing to initiation of atrial fibrillation. *Pacing Clin Electrophysiol* 2006;**29**:290–5.
21. Chen YJ, Chen SA, Chen YC, Yeh HI, Chan P, Chang MS *et al*. Effects of rapid atrial pacing on the arrhythmogenic activity of single cardiomyocytes from pulmonary veins: implication in initiation of atrial fibrillation. *Circulation* 2001;**104**:2849–54.
22. Patterson E, Po SS, Scherlag BJ, Lazzara R. Triggered firing in pulmonary veins initiated by *in vitro* autonomic nerve stimulation. *Heart Rhythm* 2005;**2**:624–31.
23. Hocini M, Ho SY, Kawara T, Linnenbank AC, Potse M, Shah D *et al*. Electrical conduction in canine pulmonary veins: electrophysiological and anatomic correlation. *Circulation* 2002;**105**:2442–8.
24. Hsieh MH, Tai CT, Tsai CF, Yu WC, Lin WS, Huang JL *et al*. Mechanism of spontaneous transition from typical atrial flutter to atrial fibrillation: role of ectopic atrial fibrillation foci. *Pacing Clin Electrophysiol* 2001;**24**:46–52.
25. Zhou S, Chang CM, Wu TJ, Miyauchi Y, Okuyama Y, Park AM *et al*. Nonreentrant focal activations in pulmonary veins in canine model of sustained atrial fibrillation. *Am J Physiol Heart Circ Physiol* 2002;**283**:H1244–52.